

Lepton collisions in MadGraph5_aMC@NLO

Stefano Frixione^{*1}, Olivier Mattelaer^{†2}, Marco Zaro^{‡3}, and Xiaoran Zhao^{§4}

¹INFN Sezione di Genova, Via Dodecaneso 33, 16146, Genova, Italy

²Centre for Cosmology, Particle Physics and Phenomenology (CP3), Université Catholique de Louvain,
Chemin du Cyclotron, 1348 Louvain la Neuve, Belgium

³TIFLab, Dipartimento di Fisica, Università degli Studi di Milano and INFN, Sezione di Milano,, Via
Celoria 16, 20133 Milano, Italy

⁴Dipartimento di Matematica e Fisica, Università di Roma Tre and INFN, sezione di Roma Tre,
I-00146 Rome, Italy

August 24, 2021

Abstract

MadGraph5_aMC@NLO is a software package that allows one to simulate processes of arbitrary complexity, at both the leading and the next-to-leading order perturbative accuracy, with or without matching and multi-jet merging to parton showers. It has been designed for, and so far primarily employed in the context of, hadronic collisions. In this note, we document the implementation of a few technical features that are necessary to extend its scope to realistic e^+e^- collider environments. We limit ourselves to discussing the unpolarized-beam case, but we point out that the treatment of polarized beams is conceptually identical, and that the structure we set up can easily be extended to carry out simulations at $\mu^+\mu^-$ colliders.

1 Introduction

In view of the fact that MADGRAPH5_AMC@NLO [1] (referred to as MG5_AMC henceforth) has not been extensively employed so far in the context of e^+e^- collisions, we give here the briefest of summary of its present scope and characteristics. MG5_AMC constructs automatically the short-distance cross section for an arbitrary process, given in input by the user together with the Lagrangian of the theory (in the form of a UFO model [2]) in which the computation is performed; such a cross section is subsequently integrated and, where appropriate, unweighted events associated with it are stored as Les Houches event (LHE henceforth) files [3, 4]. The form of the cross section depends on the type of simulation one wishes to perform, which is in turn determined by the combination of its perturbative accuracy (leading order (LO) or next-to-leading order (NLO)), of whether it is matched or not to a parton shower Monte Carlo (MC) and, in the case where such a matching is involved, whether multi-jet merging is also required. The interested reader can find full details in ref. [1].

If the underlying accuracy is an LO one, the features just described are qualitatively similar to those of the MADGRAPH family. However, it is important to keep in mind that MG5_AMC

^{*}Stefano.Frixione@cern.ch

[†]olivier.mattelaer@uclouvain.be

[‡]marco.zaro@mi.infn.it

[§]xiaoran.zhao@uniroma3.it

now vastly exceeds the capabilities of the latter codes; in particular, it supersedes their most recent ones, MADGRAPH5 [5], and must be used in its place. Conversely, at the NLO MG5_AMC collects the features developed in the course of several works – the automation [6] of the FKS [7,8] subtraction, and of the parton-shower matching (and merging) according to the MC@NLO [9] (FxFx [10]) formalism. In keeping with the general philosophy that underpins the code, the type of perturbative series is driven by the given UFO model; furthermore, MG5_AMC is capable of handling simultaneously the expansion in two coupling constants, most notably those of QCD and of the electroweak Standard Model (EW SM). The latter one is expected to be increasingly relevant as the LHC enters a high-precision phase, and it is obviously particularly important for e^+e^- computations; its (technically involved) automation has been presented in ref. [11].

What has been said thus far broadly summarises the status of MG5_AMC as a widely-used tool for hadronic-collision simulations. Remarkably, at the level of short-distance cross sections *no changes* are necessary for it to deal with the case of e^+e^- collisions, regardless of the perturbative accuracy (LO or NLO) and of the underlying theoretical model (e.g. QCD and/or EW). However, while e^+e^- short-distance cross sections (at variance with their hadronic counterparts) can give one a very good idea of the corresponding physics, strictly speaking they are non-physical as soon as one takes into account *EW-induced corrections*, owing to their lacking the description of two phenomena, namely: *a)* beamstrahlung effects¹; *b)* multiple emissions of low-energy/low-angle photons and leptons from the particles that are about to enter the hard process – such multiple emissions will be collectively called initial-state radiation (ISR) effects henceforth. We point out that only ISR, at variance with beamstrahlung, can be unambiguously classified as perturbative. More details will be given in sect. 2.

In summary, the public version of MG5_AMC could compute, before the present work, both LO- and NLO-accurate e^+e^- cross sections, but without including beamstrahlung and ISR effects. The goal of this note is to document the implementation of such effects in the code in view of its next release², that will be limited to leading-logarithmic (LL) and LO results³ in α , while no restriction will be imposed on the accuracy in α_s .

2 e^+e^- cross sections

Both beamstrahlung and ISR are due to initial-state emissions. Conventionally, all perturbative and collider-independent effects are associated with the latter, whereas the former accounts for collider-specific beam-dynamics phenomena. The evaluation of ISR effects necessarily involves an analysis to all orders in perturbation theory, and thus entails some degree of approximation. The approach we follow in MG5_AMC is based on parametrising ISR by means of a factorisation formula, quite similar to its QCD counterpart. Conversely, the understanding of beamstrahlung is rather heuristic, and typically stems from an MC simulation of beam-beam interactions, which is strictly collider dependent. Beamstrahlung and ISR are independent from each other; however, while the prediction of a physical e^+e^- cross section must include ISR effect, beamstrahlung ones might or might not be required. Therefore, in MG5_AMC two options are considered: either ISR-only, or ISR combined with beamstrahlung.

¹More precisely, beam-beam interactions, of which beamstrahlung is one of the consequences, and typically the dominant one on the energy spectra of the incoming particles. Because of this dominance, in a slightly improper manner we shall identify the two concepts in this note.

²That will be v3.2.0 of MG5_AMC. We point out that an independent implementation of ISR effects in MG5_AMC has been presented in refs. [12, 13]. The latter have a limited scope, and are superseded by the present work.

³This strictly applies to the code implementation: the formulae presented in this note are general, and encompass all cases. The code will soon be upgraded to included higher-order effects in α .

Following ref. [14], we write the differential cross section for the production of a system of particles X in e^+e^- collisions:

$$e^+(P_{e^+}) + e^-(P_{e^-}) \longrightarrow X \quad (1)$$

as follows:

$$d\Sigma_{e^+e^-}(P_{e^+}, P_{e^-}) = \sum_{kl} \int dy_+ dy_- \mathcal{B}_{kl}(y_+, y_-) d\sigma_{kl}(y_+ P_{e^+}, y_- P_{e^-}), \quad (2)$$

with

$$k \in \{e^+, \gamma\}, \quad l \in \{e^-, \gamma\}, \quad (3)$$

and where the sum over polarisation states is understood. In eq. (2), the function $\mathcal{B}_{kl}(y_+, y_-)$ parametrises the emergence of the pair of particles k and l due to the dynamics of the incoming e^+e^- beams. Such two particles carry a fraction (equal to y_+ and y_- , respectively) of the longitudinal momentum of the incoming beams. In turn, particles k and l undergo a hard collision, whose cross section is denoted by $d\sigma_{kl}$ and which includes ISR effects. The ranges of their possible identities in eq. (3) stem from considering only the dominant contributions to the vast majority of production processes; they can be extended if need be. As was anticipated, we parametrise $d\sigma_{kl}$ by writing the cross section as follows:

$$\begin{aligned} d\sigma_{kl}(p_k, p_l) &= \sum_{ij} \int dz_+ dz_- \Gamma_{i/k}(z_+, \mu^2, m^2) \Gamma_{j/l}(z_-, \mu^2, m^2) \\ &\quad \times d\hat{\sigma}_{ij}(z_+ p_k, z_- p_l, \mu^2, m^2). \end{aligned} \quad (4)$$

In eq. (4), the $\Gamma_{i/k}$ symbol denotes the PDF of *parton* i in *particle* k ; the former carries a fraction z_{\pm} of the longitudinal momentum of the latter. Such a quantity is thus conceptually similar to its QCD counterpart, and indeed it obeys the same DGLAP [15–18] evolution equations⁴:

$$\frac{\partial \Gamma_{i/k}}{\partial \log \mu^2} = \frac{\alpha}{2\pi} P_{ij} \otimes \Gamma_{j/k}. \quad (5)$$

Importantly, the PDFs of interest here can be fully computed in a perturbative manner, at variance with the QCD ones. The quantity denoted by $d\hat{\sigma}_{ij}$ in eq. (4) is the (IR-subtracted) partonic short-distance cross section, associated with the following hard process:

$$i(z_+ p_k) + j(z_- p_l) \longrightarrow X. \quad (6)$$

Finally, by m and μ we have denoted the electron mass and a scale of the order of the hardness of the process. In MG5_AMC, the latter can be set by the user. While for full generality in eq. (4) we have included an electron-mass dependence in the partonic cross section, in practice in MG5_AMC such a dependence is always ignored: all electron-mass effects are included by means of the PDFs (analogous final-state effects would have to be included by means of fragmentation functions).

In summary, the physics content of eq. (2), and our naming conventions for it, can be compactly written as follows:

$$\text{beams} \xrightarrow{\text{beamstrahlung}} \text{particles} \xrightarrow{\text{ISR}} \text{partons}. \quad (7)$$

Consistently with this, we call:

⁴We limit ourselves to only including QED effects in our ISR parametrisation. If need be, purely-weak ones can be accounted for with the same formalism.

- $d\Sigma_{e^+e^-}$: collider-level cross section.
- $d\sigma_{kl}$: particle-level cross section.
- $d\hat{\sigma}_{ij}$: (subtracted) parton-level cross section.

Note that, at variance with the QCD case, the identities of a particle and of a parton might coincide (in particular, the PDF of an electron/positron in an electron/positron will generally give the dominant contributions at an e^+e^- collider).

According to eq. (3), one or two photons might emerge from the beamstrahlung and initiate the hard process. In practice, in the current version of MG5_AMC we limit ourselves to considering the case $(k, l) = (e^+, e^-)$ – in other words, the identities of the particles coincide with those of the beams whence they emerge; formally:

$$\mathcal{B}_{kl}(y_+, y_-) = \delta_{ke^+} \delta_{le^-} \mathcal{B}_{e^+e^-}(y_+, y_-). \quad (8)$$

Conversely, the identities of the partons are dictated by the combination of the nature of the system X , of the required perturbative accuracy, and of the (formal) perturbative expansions of the partonic cross sections and of the PDFs. At the LO in α (i.e. the only option we make publicly available as a result of the present work) this is trivial, as it only involves electrons/positrons. We shall specify in a future note the strategy we shall pursue when dealing with higher-order QED corrections.

The current public version of MG5_AMC is able to compute partonic cross sections. In this note, we document the implementation of the beamstrahlung and ISR effects according to eqs. (2) and (4), respectively, within the assumptions discussed above.

3 ISR

As was anticipated in sect. 2, we currently ignore the particle-level cross sections which are not initiated by an e^+e^- pair. Therefore, we implement eq. (4) with $(k, l) = (e^+, e^-)$ and can thus limit ourselves to employing electron PDFs (see footnote 4). For such PDFs, in MG5_AMC the choice is given to adopt either the LO+LL results of refs. [19–21] or (in future versions) the NLO+NLL ones of refs. [22, 23]; more details on these PDFs can be found in those papers.

The structure of eq. (4) is the same as that of the factorisation theorems of QCD, upon which the simulations of hadronic collisions in MG5_AMC is based. Unfortunately, the corresponding implementation cannot be used as is in the context of e^+e^- collisions, owing to the vastly different behaviour of hadron and electron PDFs – while the former peak at small z 's, the latter peak at $z \rightarrow 1$. Furthermore, while in hadronic collisions the very-small- z integration region is cut-off by the requirement that there be a minimal invariant mass produced by the hard process, in e^+e^- collisions the region around $z = 1$ is never cut-off; it actually gives the dominant contribution to the cross section by far⁵. This is due to the fact that the PDF of an electron/positron in an electron/positron reads as follows in the $z \rightarrow 1$ region:

$$\Gamma_{e^\pm/e^\pm}(z) \xrightarrow{z \rightarrow 1} \frac{\hat{\Gamma}_{e^\pm/e^\pm}(z)}{(1-z)^{1-\beta}} \quad (9)$$

both at the LO+LL and at the NLO+NLL (see refs. [22, 23]). The function $\hat{\Gamma}_{e^\pm/e^\pm}(z)$ is at most logarithmically-divergent at $z \rightarrow 1$, and β is a parameter whose precise definition (and

⁵The presence of an s -channel resonance with mass smaller than the collider energy can partly act as an effective cut-off; we shall discuss this case in the following.

possible dependence on the hard scale of the process) depends on the perturbative order, but which is always numerically small (at the typical e^+e^- colliders considered nowadays, $\beta \simeq 0.05$). Thus, eq. (9) exhibits a very pronounced integrable divergence at $z = 1$, which is reason for the dominance mentioned before. Conversely, the PDFs Γ_{γ/e^\pm} and Γ_{e^\mp/e^\pm} that potentially appear in an NLO computation are at most logarithmically divergent at $z \rightarrow 1$. Therefore, in the following we shall discuss only eq. (9) which, in addition to being the only one relevant to LO computations, is also a worst-case scenario.

In order to integrate eq. (4) with PDFs that behave as in eq. (9), MG5_AMC performs e^+e^- -specific changes of variables. One starts by writing the PDFs as follows:

$$\Gamma_{e^\pm/e^\pm}(z) = \frac{\bar{\Gamma}_{e^\pm/e^\pm}(z)}{(1-z)^\gamma}, \quad (10)$$

with γ a free constant parameter such that:

$$1 - \beta \leq \gamma < 1. \quad (11)$$

Note that, owing to the smallness of β , γ must always be chosen rather close to one. This implies that the functions $\bar{\Gamma}_{e^\pm/e^\pm}(z)$ implicitly defined in eq. (10) are at most logarithmically divergent at $z = 1$ when $\gamma = 1 - \beta$, and vanish there otherwise. Then, one introduces the variables:

$$t_\pm = \left(\frac{1 - z_\pm}{1 - z_{0\pm}} \right)^{1-\gamma} \implies \frac{dz_\pm}{dt_\pm} = \frac{1 - z_{0\pm}}{1 - \gamma} t_\pm^{\gamma/(1-\gamma)} = \frac{(1 - z_{0\pm})^{1-\gamma}}{1 - \gamma} (1 - z_\pm)^\gamma, \quad (12)$$

with $z_{0\pm} \geq 0$ the lower limit of the integration range in z_\pm . Thus, for each of the two incoming-particle legs:

$$\begin{aligned} dz_\pm \Gamma_{e^\pm/e^\pm}(z_\pm) f_\pm(z_\pm) &\equiv dz_\pm \frac{\bar{\Gamma}_{e^\pm/e^\pm}(z)}{(1-z)^\gamma} f_\pm(z_\pm) \\ &= dt_\pm \bar{\Gamma}_{e^\pm/e^\pm}(z_\pm(t_\pm)) f_\pm(z_\pm(t_\pm)) \frac{(1 - z_{0\pm})^{1-\gamma}}{1 - \gamma}, \end{aligned} \quad (13)$$

where f_\pm are arbitrary regular functions. Further changes of variables $t_\pm \rightarrow u_\pm$ with:

$$t_\pm = u_\pm^k \implies \frac{dt_\pm}{du_\pm} = k u_\pm^{k-1} \quad (14)$$

and $k \gtrsim 2$ help the convergence in the case of NLO+NLL PDFs which, in the $\overline{\text{MS}}$ scheme, feature $\log^p(1-z)$ terms (whereas they do not in the scheme introduced in ref. [23], at least when the initial scale for the evolution is set equal to the electron mass).

The r.h.s. of eq. (13) is now well-behaved at $z \rightarrow 1$, and can easily be integrated numerically⁶. However, for this to happen it is crucial that $\bar{\Gamma}_{e^\pm/e^\pm}(z)$ be well behaved for all z 's, in particularly for those arbitrarily close to one⁷. For this reason, the factor

$$\frac{(1-z)^\gamma}{(1-z)^{1-\beta}} = (1-z)^{\gamma+\beta-1} \quad (15)$$

which is present in the $z \rightarrow 1$ expression of $\bar{\Gamma}_{e^\pm/e^\pm}(z)$ must always be computed as in the r.h.s. of eq. (15), and not as in its l.h.s.; in turn, this requires the analytical knowledge of the large- z

⁶Roughly speaking, the dominant $z \rightarrow 1$ integral contributions are turned into the large $1/(1-\gamma)$ factors.

⁷It is instructive to point out that the integration of eq. (4) with $d\hat{\sigma}_{ij} = 1$ and the constraint $z_+ z_- \leq 1 - 10^{-\kappa}$ is within 0.1% of its asymptotic $\kappa = \infty$ value for $\kappa = \mathcal{O}(50)$. This figure is so large that even the simple computation of $1 - z$, let alone anything more complicated than that, turns out to be beyond the accuracy of standard double-precision computations.

behaviour of the PDFs. These observations have been taken into account when the results for the (N)LO+(N)LL PDFs of refs. [22, 23]) have been implemented in numerical routines; those return $\bar{\Gamma}_{e^\pm/e^\pm}(z)$ (and not $\Gamma_{e^\pm/e^\pm}(z)$), given γ , z , and $1 - z$; the latter quantity is computed in MG5_AMC not as such, but directly as the t 's of eq. (12), for the reasons explained in footnote 7.

Given eqs. (11) and (15), it appears that the ideal choice for γ is to set it equal to $1 - \beta$. Unfortunately, this is impossible beyond LO, in view of the fact that β generally becomes scale-dependent. Since the scale may be chosen on an event-by-event basis (i.e. as a function of the kinematical configuration) in keeping with the standard assumptions in MG5_AMC, the value of β is known only after having generated the partonic four-momenta, that in turn require the variables z_\pm to have been already computed. Thus, by setting $\gamma = 1 - \beta$ one is led to a circular argument.

We conclude this part by giving a few more details on the integration ranges of the z_\pm variables. The partonic cross section on the r.h.s. of eq. (4) implicitly implements a cut-off:

$$\tau \geq \tau_0, \quad \tau = z_+ z_-, \quad \tau_0 = \frac{M_{\text{low}}^2}{(p_k + p_l)^2}, \quad (16)$$

with M_{low}^2 the smallest possible invariant mass of the system X produced in the hard collision (such a quantity is strictly larger than zero). We can thus set:

$$z_{0+} = \tau_0, \quad z_{0-} = \frac{\tau_0}{z_+}. \quad (17)$$

The asymmetric choice of eq. (17) is not ideal for analytical differential calculations. In particular, if $z_+ \rightarrow \tau_0$ then z_- will always be in a neighbourhood of one; thus, *small* z_+ values induce a sensitivity to the large- z (divergent) behaviour of the PDFs. This fact does not turn out to be problematic in numerical computations, provided that one follows the strategy outlined so far. In particular, if $z_+ \rightarrow \tau_0$ the integration range in z_- becomes vanishingly small, which is accounted for (in a numerically-stable way, when expressing z_+ in terms of t_+) by the factor $(1 - z_{0-})^{1-\gamma}$ in eq. (12).

3.1 The case of s -channel resonances

The integration procedure described above does not perform well in the presence of s -channel resonances that emerge from the incoming particles. In order to present the strategy employed by MG5_AMC in such a case, we start by observing that the problem can always be treated as if there were only one resonance. In fact, in the case of multiple resonances MG5_AMC is able to disentangle them by means of a multi-channeling strategy (see refs. [6, 24] for the LO and NLO approaches, respectively), and to treat them separately.

We denote by M and Γ the mass and the width, respectively, of the resonance of interest, and by:

$$s = (P_{e^+} + P_{e^-})^2 \quad (18)$$

the collider c.m. energy squared⁸. In view of eq. (16), we also introduce the auxiliary quantities:

$$\tau_M = \frac{M^2}{s}, \quad \tau_\Gamma = \frac{\Gamma^2}{s}. \quad (19)$$

We assume that $M < \sqrt{s}$ (since otherwise the resonance does not entail any special treatment), and therefore τ_M belongs to the integration range of $z_+ z_-$. Thus, in terms of τ the integrand of eq. (4) has two peaks, at $\tau = \tau_M$ (stemming from the s -channel resonant propagator, which

⁸This coincides with the particle c.m. energy squared when beamstrahlung effects are ignored.

gives rise to a Breit-Wigner function in the partonic cross sections) and at $\tau = 1$ (stemming from the PDFs). These are competing effects, and in order to integrate both of them efficiently, we proceed as follows. We first introduce the quantities:

$$f_{\text{res}} = \frac{1}{(\tau - \tau_M)^2 + \tau_M \tau_\Gamma}, \quad (20)$$

$$f_{\text{nr}} = \frac{1}{(1 - \tau)^{1-2\beta}}. \quad (21)$$

Equation (20) is nothing but a rescaled Breit-Wigner function, whereas the form of eq. (21) is motivated by the observation that the presence of a resonance induces an effective luminosity strongly peaked at $\tau = 1$:

$$\mathcal{L}(\tau) = \int dz_+ dz_- \delta(\tau - z_+ z_-) \Gamma_{e^+e^+}(z_+) \Gamma_{e^-e^-}(z_-) \xrightarrow{\tau \rightarrow 1} \frac{1}{(1 - \tau)^{1-2\beta}}, \quad (22)$$

where use of eq. (9) has been made. The current integration channel is then split into two terms, by multiplying the partonic cross section by a factor equal to one, written as follows:

$$1 = F_{\text{res}} + F_{\text{nr}}, \quad (23)$$

with:

$$F_{\text{res}} = \frac{f_{\text{res}}}{f_{\text{res}} + f_{\text{nr}}}, \quad (24)$$

$$F_{\text{nr}} = \frac{f_{\text{nr}}}{f_{\text{res}} + f_{\text{nr}}}. \quad (25)$$

In other words, the r.h.s. of eq. (4) is written as the sum of two terms, each of which identical to the r.h.s. of eq. (4) bar for the insertion of either F_{res} or F_{nr} in the integrand. Such terms are then integrated separately⁹. For the one relevant to F_{nr} we proceed as was explained in sect. 3, while for that relevant to F_{res} we first change integration variables $(z_+, z_-) \rightarrow (\tau, z_i)$, with either $z_i = z_+$ or $z_i = z_-$ (chosen at random, and exploiting the fact that at the LO+LL the situation of the two beams is symmetric). Next, we flatten the integration in τ by generating it by means of the inverse of the integral function of eq. (20), and that in z_i by using the change of variables of eq. (12).

4 Beamstrahlung

We now consider the case of a non-trivial beamstrahlung function in eq. (2); it is in fact possible to treat such a case in the same formal way as the trivial one (i.e. as if beamstrahlung were not present), since the latter corresponds to setting:

$$\mathcal{B}_{kl}(y_+, y_-) = \delta_{ke} \delta_{le} \delta(1 - y_+) \delta(1 - y_-). \quad (26)$$

As we shall see the similarity between the trivial and non-trivial cases is even stronger, since non-trivial beamstrahlung functions feature combinations of regular functions and of distributions.

As was said above, information on the beamstrahlung function is obtained by means of MC simulations: codes able to perform such simulations include CAIN [25], GuineaPig [26],

⁹In practice, this is done on the fly. We generate a random number r ; if $r < r_M$ ($r > r_M$) we integrate the F_{res} (F_{nr}) term. The value of r_M can be set either in an adaptive manner, or fixed (e.g. $r_M = 1/2$), the two choices being conceptually equivalent to each other.

and GuineaPig++ [27]. The format in which the results of the MC simulations are stored in order for the cross-section integrators to use them is not standard, and one should employ the structure best suited to one own's needs. For example, in CIRCE1 [28] a beta function is adopted to fit the one-dimensional energy spectrum for each beam, thereby ignoring correlations between the two beams. Such an approach has later been extended [29] to a two-dimensional fit that allows one to account for beam correlations. Conversely, in CIRCE2 [30] a grid-based strategy is adopted instead.

A peculiar characteristics of eq. (2), as opposed to its particle-level counterpart eq. (4), is that the beamstrahlung functions $\mathcal{B}_{kl}(y_+, y_-)$ are not separable in their arguments y_{\pm} . We must therefore use the fact that the following representation holds [29]:

$$\mathcal{B}_{kl}(y_+, y_-) \approx \sum_{n=1}^N b_{n,kl}^{(e^+)}(y_+) b_{n,kl}^{(e^-)}(y_-), \quad (27)$$

for suitable basis functions $b_{n,kl}^{(e^{\pm})}(y)$. Equation (27) becomes an identity for $N \rightarrow \infty$, but in practice one can obtain a highly accurate representation of \mathcal{B}_{kl} even with a relatively small value of N . In particular, for the only case $((k, l) = (e^+, e^-))$, see eq. (8)) implemented in MG5_AMC v3.2.0, we have found the following form to give satisfactory results for both linear and circular colliders¹⁰:

$$\begin{aligned} \mathcal{B}_{e^+e^-}(y_+, y_-) &= \hat{f}_{11} \delta(1 - y_+) \delta(1 - y_-) \\ &+ (1 - y_+)^{\kappa_+} f_{01}(y_+) \delta(1 - y_-) \\ &+ \delta(1 - y_-) (1 - y_-)^{\kappa_-} f_{10}(y_-) \\ &+ (1 - y_+)^{\kappa_+} f_{00+}(y_+) (1 - y_-)^{\kappa_-} f_{00-}(y_-), \end{aligned} \quad (28)$$

with [31]

$$\kappa_+ = \kappa_- = -2/3, \quad (29)$$

and where the functions $f_{\alpha}(y)$ are regular, and generally depend on the collider type. By equating the r.h.s.'s of eqs. (27) (with $N = 4$) and (28) one can solve for the functions $b_{n,e^+e^-}^{(e^{\pm})}(y_{\pm})$ that appear in the former; we need not do it explicitly here. The complete determination of $\mathcal{B}_{e^+e^-}(y_+, y_-)$ is achieved by choosing suitable forms for the functions $f_{\alpha}(y)$, that depend on a finite number of parameters. After having done that, beam dynamics is simulated by means of GuineaPig [26] with high-statistics runs (with up to 100M events). The results of these are first separated according to whether the condition(s) $y_{\pm} = 1$ is(are) met, then when either $y_+ \neq 1$ and/or $y_- \neq 1$ are histogrammed in the y_+ and/or y_- variables, and subsequently fit separately with the last three lines of eq. (28), in order to determine the free parameters of the chosen functional forms. Conversely, the \hat{f}_{11} parameter is simply determined by the counting of events with $y_+ = 1$ and $y_- = 1$. It is clear that this operation, while time-consuming, must be done only once per collider type. We have considered several examples; these are summarised in table 1, which also reports the values of the beam-dynamics parameters used in the GuineaPig simulations.

In order to be more specific, let us first consider the case of circular colliders. By means of the function

$$f(y; p, q) = e^{p(1-y)} e^{q\sqrt{1-y}} \quad (30)$$

¹⁰We assume $0 \leq y_{\pm} \leq 1$, and therefore ignore beam-spread effects.

	Name [26]	FCC-ee	CEPC	ILC	CLIC
$E_{beam}[\text{GeV}]$	energy	120, 182.5	120	125, 250	1500
$N[10^{10}]$	particles	15, 27	15	2	0.37
$\sigma_E[10^{-3}]$	espread	1.65, 2.0	1.0	$[e^-:1.9,1.2][e^+:1.5,0.7]$	3.5
$\sigma_x[\text{nm}]$	sigma_x	14000, 38000	21000	520, 470	40
$\sigma_y[\text{nm}]$	sigma_y	40, 70	70	8, 6	1
$\sigma_z[\mu\text{m}]$	sigma_z	5300, 3800	3300	300	44
$\beta_x[\text{mm}]$	beta_x	300, 1000	360	13, 22	6.9
$\beta_y[\text{mm}]$	beta_y	1, 1.6	1.5	0.41, 0.48	0.068
$\theta[\text{rad}]$	angle_x	0.015	0.0165	0.007	0.010

Table 1: e^+e^- collider configurations, with the respective parameters used in the GuineaPig simulations: E_{beam} is the beam energy, N the number of particles per bunch, σ_E the beam-energy spread, σ_x, σ_y the beam sizes, σ_z the bunch length, β_x, β_y the amplitude functions, and θ the crossing angle.

we set:

$$f_{01}(y) = \hat{f}_{01} f(y; p_{01}, q_{01}), \quad (31)$$

$$f_{10}(y) = \hat{f}_{10} f(y; p_{10}, q_{10}), \quad (32)$$

$$f_{00+}(y) = \hat{f}_{00+} f(y; p_{00+}, q_{00+}), \quad (33)$$

$$f_{00-}(y) = \hat{f}_{00-} f(y; p_{00-}, q_{00-}). \quad (34)$$

The values of the parameters \hat{f}_i , p_i , and q_i that result from the fits to the GuineaPig simulations as described above are reported in tables 2, 3, and 4 for the circular-collider configurations of table 1, namely FCC-ee with $E_{beam} = 120$ GeV (denoted by FCC-ee240), FCC-ee with $E_{beam} = 182.5$ GeV (denoted by FCC-ee365), and CEPC with $E_{beam} = 120$ GeV (denoted by CEPC240), respectively. The corresponding comparisons between the fitted functional forms and the simulation data are presented in appendix A, in figs. 1 and 2, 3 and 4, and 5 and 6.

i	\hat{f}_i	p_i	q_i	Integral
11	0.8698			
01	0.2863	-901.2	-19.30	0.06234
10	0.2853	-916.5	-18.70	0.06230
00+	0.3308	-899.2	-18.03	0.07308
00-	0.3303	-918.7	-17.48	0.07306
Sum				0.9998

Table 2: Fit results for FCC-ee240.

Turning to the cases of the linear-collider configurations of table 1, the values of the parameters resulting from the fits are reported in tables 5, 6, and 7 for ILC with $E_{beam} = 125$ GeV (denoted by ILC250), ILC with $E_{beam} = 250$ GeV (denoted by ILC500), and CLIC with $E_{beam} = 1500$ GeV (denoted by CLIC3000), respectively. The corresponding comparisons between the fitted functional forms and the simulation data are presented in appendix A, in figs. 7 and 8, 9 and 10, and 11 and 12.

We point out that the general functional form that we employ for the fits at linear colliders is still that of eq. (28), with eq. (29) and eqs. (31)–(34). However, while for ILC250 we adopt

i	\hat{f}_i	p_i	q_i	Integral
11	0.7883			
01	0.4056	-714.3	-14.64	0.09856
10	0.4059	-714.5	-14.69	0.09856
00+	0.4772	-714.7	-12.77	0.1188
00-	0.4780	-717.1	-12.80	0.1189
Sum				0.9996

Table 3: Fit results for FCC-ee365.

i	\hat{f}_i	p_i	q_i	Integral
11	0.8351			
01	0.3513	-910.9	-17.28	0.07806
10	0.3515	-914.2	-17.27	0.07803
00+	0.4075	-917.9	-15.44	0.09230
00-	0.4080	-918.8	-15.45	0.09239
Sum				0.9997

Table 4: Fit results for CEPC240.

i	\hat{f}_i	p_i	q_i	Integral
11	0.4933			
01	0.2085	-21.17	-0.01452	0.2016
10	0.2085	-21.19	-0.01460	0.2016
00+	0.3259	-20.22	-0.01416	0.3200
00-	0.3263	-20.25	-0.01420	0.3203
Sum				0.9990

Table 5: Fit results for ILC250.

i	\hat{f}_i	p_i	q_i	Integral
11	0.5012			
01	0.1613	-8.514	-5.808	0.1983
10	0.1613	-8.505	-5.823	0.1983
00+	0.2528	-7.535	-6.790	0.3173
00-	0.2524	-7.481	-6.849	0.3171
Sum				0.9985

Table 6: Fit results for ILC500.

eq. (30), for ILC500 and CLIC3000 we use:

$$f(y; p, q) = e^{p(1-y)} e^{q(1-y)^{3/2}}, \quad (35)$$

$$f(y; p, q) = e^{p(1-y)} e^{qy^{-3/2}}, \quad (36)$$

respectively, in view of the stronger beamstrahlung effects at these colliders.

Owing to the symmetry between the two beams enforced by eq. (8) in the current implementation of MG5_AMC, we could have decided to use the same parameters for the functions relevant

i	\hat{f}_i	p_i	q_i	Integral
11	0.7434			
01	0.04563	-0.6016	-0.007179	0.1162
10	0.04568	-0.6089	-0.007135	0.1162
00+	0.05943	-0.5629	-0.007464	0.1524
00-	0.05951	-0.5743	-0.007259	0.1523
Sum				0.9990

Table 7: Fit results for CLIC3000.

to the y_+ and y_- variables, namely to set $\hat{f}_i = \hat{f}_j$, $p_i = p_j$, and $q_i = q_j$ for $(i, j) = (01, 10)$ and $(i, j) = (00+, 00-)$ prior to fitting. We have chosen not to do so, and rather verify that such identities are (approximately) fulfilled post-fit; this constitutes a check on the general correctness of the fitting procedure. Another check is the unitarity of the luminosity, namely that the integral of the $\mathcal{B}_{e^+e^-}(y_+, y_-)$ function must be equal to one¹¹. In tables 2–7 we report, in the columns labelled as “Integral”, the integrals of the $(1 - y_{\pm})^{\kappa_{\pm}} f_i(y_{\pm})$ functions. The sum of the result for $i = 01$, plus that for 10, plus the product of those for 00+ and 00-, plus the value of \hat{f}_{11} , reported in the tables as “Sum”, gives the sought normalised luminosity. As we see, that number is always very close to one.

The check on the unitarity of the luminosity guarantees that the fits behave as expected in the regions $y_{\pm} \simeq 1$, which give by far the dominant contributions to the physical cross sections. The quality of the fits can also be assessed in a fully local way, by comparing them to the simulation data, as is done in the figures we report in appendix A. As we see there, at circular colliders there is a tendency for the fits to undershoot the data as small y_{\pm} values are approached. While this should be a minor problem in the computation of observables (owing to the extremely small value assumed by the beamstrahlung function in those regions), we stress that our framework for fitting $\mathcal{B}_{e^+e^-}(y_+, y_-)$ is fully flexible, and can easily accomodate functions more involved than those of eqs. (30), (35), and (36).

5 ISR and beamstrahlung

The separation of variables introduced in eq. (27) allows one to define functions that include the parametrisation of both beamstrahlung and ISR effects. Indeed, it is straightforward to see that eqs. (2) and (4) lead to¹²:

$$\begin{aligned}
d\Sigma_{e^+e^-}(P_{e^+}, P_{e^-}) &= \sum_{n=1}^N \sum_{ijkl} \int dx_+ dx_- \phi_{i/k,n,kl}^{(e^+)}(x_+, \mu^2, m^2) \phi_{j/l,n,kl}^{(e^-)}(x_-, \mu^2, m^2) \\
&\quad \times d\hat{\sigma}_{ij}(x_+ P_{e^+}, x_- P_{e^-}, \mu^2, m^2),
\end{aligned} \tag{37}$$

where:

$$\phi_{i/k,n,kl}^{(e^{\pm})}(x, \mu^2, m^2) = \int dy dz \delta(x - yz) b_{n,kl}^{(e^{\pm})}(y) \Gamma_{i/k}(z, \mu^2, m^2). \tag{38}$$

While eq. (37) is equivalent to the combination of eqs. (2) and (4), it gives one the possibility of computing a collider-level cross section in an alternative way w.r.t. to the latter two. This

¹¹We normalise the GuineaPig simulations to the total number of events.

¹²Equation (37) is fully general. In keeping with the characteristics of the present implementation (see eq. (28)), in the code we set $(k, l) = (e^+, e^-)$.

is because the quantities introduced in eq. (38) depend only on the collider type (through the beamstrahlung function) and on the small-angle initial state radiation (through the PDFs). In other words, they are process *independent*, and as such can be parametrised once and for all.

We exploit this fact in the following way. Firstly, the leading $x \rightarrow 1$ behaviour of the functions on the l.h.s. of eq. (38) can be analytically computed if the same kind of information is available for the functions in the integrand on the r.h.s. of eq. (38), which is the case (see eq. (28) and refs. [22, 23]). The worst-case scenario is again that relevant to electron/positron PDFs, as was already pointed out in sect. 3. By using eq. (9) one immediately arrives at:

$$\phi_{e^\pm/e^\pm, n, e^+e^-}^{(e^\pm)}(x) \xrightarrow{x \rightarrow 1} \frac{\hat{\phi}_{e^\pm/k, n, e^+e^-}^{(e^\pm)}(x)}{(1-x)^{1-\beta}} \quad \text{if} \quad b_{n, e^+e^-}^{(e^\pm)}(y) \propto \delta(1-y), \quad (39)$$

$$\phi_{e^\pm/e^\pm, n, e^+e^-}^{(e^\pm)}(x) \xrightarrow{x \rightarrow 1} \frac{\hat{\phi}_{e^\pm/k, n, e^+e^-}^{(e^\pm)}(x)}{(1-x)^{-\kappa-\beta}} \quad \text{if} \quad b_{n, e^+e^-}^{(e^\pm)}(y) \propto (1-y)^\kappa. \quad (40)$$

Thus, we introduce the analogue of eq. (10) as follows:

$$\phi_{i/k, n, kl}^{(e^\pm)}(x) = \frac{\bar{\phi}_{i/k, n, kl}^{(e^\pm)}(x)}{(1-x)^{\bar{\kappa}}}, \quad (41)$$

and construct routines that, given the beamstrahlung functions and the PDFs, return the $\bar{\phi}_\alpha$ functions and the coefficient $\bar{\kappa}$. In order to do this, we need to bear in mind the discussion presented in sect. 3 about the $z \rightarrow 1$ behaviour of the PDFs, and the necessity of employing the free parameter γ , in order to be able put the LO+LL and NLO+NLL PDFs on the same footing. For the examples of eqs. (39) and (40), we have:

$$\text{eq. (39)} \quad \longrightarrow \quad \bar{\kappa} = \gamma, \quad (42)$$

$$\text{eq. (40)} \quad \longrightarrow \quad \bar{\kappa} = \gamma - 1 - \kappa. \quad (43)$$

For what concerns the functions $\bar{\phi}_\alpha$, the integral in eq. (38) is computed for several pre-defined values of the pair (x, μ^2) – such values thus constitute the nodal points of a two-dimensional grid. The integral results are written in a file, together with a routine that reads them and, by using the information on the nodal points as well, returns the sought functions for any arbitrary values of x and μ^2 by performing a bi-linear interpolation of the stored results. Since the functions $\bar{\phi}_\alpha$ are well-behaved in the whole x range (thanks to the factor $(1-x)^{\bar{\kappa}}$ introduced in eq. (41)), the procedure just outlined is sufficient to achieve a satisfactory level of precision. In particular, for the numerical tests performed so far, which are restricted to LO+LL results, we have used the nodal points obtained with 100 x values (distributed according to a polynomial law that accumulates relatively more points towards $x = 0$ and $x = 1$) and 20 μ^2 values (distributed linearly in $\log \mu^2$ in the range $\mu \in [1, 10^4]$ GeV), but we stress that these are input parameters to the code that constructs the interpolating grids, and can thus be changed at will. Such a code will be distributed with MG5_AMC, in order to allow the user to construct his/her own $\bar{\phi}_\alpha$ functions specific for the e^+e^- collider of interest.

Having parametrised once and for all the functions $\phi_{i/k, n, kl}^{(e^+)}$, eq. (37) is exactly on the same footing as eq. (4), and therefore the same strategy described in sect. 3 for the integration of the particle cross section can be used to obtain the collider-level cross section. In principle, this observation applies to each of the summands in the index n that appear in eq. (37). However, we have so far found no loss of accuracy by treating all of those terms with the same change of variables, which is dictated by the worst-case scenario $\bar{\kappa} = \gamma$. The advantage of this is that one

can use the luminosity function

$$\sum_{n=1}^N \phi_{i/k,n,kl}^{(e^+)}(x_+, \mu^2, m^2) \phi_{j/l,n,kl}^{(e^-)}(x_-, \mu^2, m^2) \quad (44)$$

as a single number that multiplies that partonic cross section (in view of the fact that the latter is n -independent); this implies that the number of integration channels for a collider-level cross section is the same as that relevant to the corresponding particle cross section. Having said that, we stress that the separate treatment of the contributions to eq. (37) associated with different n values is a pure matter of implementation, without any conceptual implications.

We conclude this section with an observation on the calculation of collider-level cross sections. Equation (37) is identical to eq. (2), where the particle cross section in the latter equation is computed with eq. (4). However, from the numerical viewpoint eq. (2) entails the generation of two extra integration variables w.r.t. what happens with eq. (37) – with the former, one needs to generate y_{\pm} and z_{\pm} , while for the latter only x_{\pm} are generated. This happens thanks to the pre-tabulation of the ϕ_{α} functions; in other words, one trades the generation of two integration variables in the context of cross-sections runs for the generation of two variables in the pre-tabulation phase, i.e. prior to physics runs. This is clearly helpful in reducing the complexity of the calculations, and thus in achieving a faster convergence for a given accuracy target. The only possible drawback of adopting eq. (37) is that by doing so the event-by-event information on the incoming-particle energies are lost; they can however be recovered on statistical basis, by randomly generating (for each of two incoming legs) the variable y that appear in eq. (38) according to its distribution as defined by the integrand on the r.h.s. of that equation.

6 Running the code

The generic instructions to run MG5_AMC have been described elsewhere (see e.g. refs. [1, 11]). Here we limit ourselves to discussing those specific to lepton-lepton collisions.

The process generation and output stages are unchanged w.r.t. the current usage. The code can be run in either the LO or the NLO-QCD mode; the NLO-EW mode is not yet supported. At the NLO in QCD, both fixed-order (fNLO) and parton-shower matched computations (NLO+PS) are supported; in the latter case, the user may also enable QED showers (this does not imply any QED matching, given that the underlying matrix elements are restricted to being of LO in the EW coupling constant). Prior to running the code, the user must specify in `run_card.dat` that ISR and possibly beamstrahlung are to be included. This is done by means of the `lpp1` and `lpp2` variables, which must be set equal to +3 (−3) for an electron (positron) beam. Parameterisations of ISR (plus possibly beamstrahlung) effects, as described in sects. 3–5, are provided as tabulated fortran files, stored in the directories `Source/PDF/lep_densities/XXX/`. Here `XXX` denotes a specific choice of ISR(+beamstrahlung) parametrisation. The options included in the code release are `XXX=isronly11` (for the LL+LO electron/positron PDFs), `cepc24011`, `clic300011`, `fcce24011`, `fcce36511`, and `ilc50011` (for the beamstrahlung configurations described in sect. 4 convoluted with the LL+LO PDFs). For reasons of benchmarking and compatibility with results in the literature, the following form for the LL+LO electron/positron PDFs is presently adopted:

$$\Gamma_{e^{\pm}/e^{\pm}}(z) = \frac{e^{3\beta/4-\gamma_E\beta}}{\Gamma(1+\beta)} \beta(1-z)^{\beta-1} - \frac{\beta}{2} h_1(z) - \frac{\beta^2}{8} h_2(z), \quad (45)$$

$$h_1(z) = 1 + z, \quad (46)$$

$$h_2(z) = \frac{1+3z^2}{1-z} \ln(z) + 4(1+z) \ln(1-z) + 5 + z, \quad (47)$$

where

$$\beta = \frac{\alpha}{\pi} \left(\log \frac{\mu^2}{m^2} - 1 \right). \quad (48)$$

At the later stage, we shall implement all options stemming from refs. [22,23]. The user’s choice of the ISR(+beamstrahlung) parametrisation are set in `run_card` by means of the assignment `pdlabel=XXX`. New ISR(+beamstrahlung) scenarios can be added by creating a new directory under `Source/PDF/lep_densities` as discussed before; this must contain exactly two files named `eepdf.f` and `gridpdfaux.f`, using the formats of those present in one of the directories already available.

Acknowledgments

M.Z. is supported by the “Programma per Giovani Ricercatori Rita Levi Montalcini”, granted by the Italian Ministero dell’Università e della Ricerca (MUR). X.Z. is supported by the Italian Ministry of Research (MUR) under grant PRIN 20172LNEEZ. The work of O.M. and of X. Z. has been supported in part by the European Union’s Horizon 2020 research and innovation programme as part of the Marie Skłodowska-Curie Innovative Training Network MCnetITN3 (grant agreement no. 722104). The authors thank Fabio Maltoni for comments on the manuscript.

A Fit results

In this appendix we complement the information, reported in sect. 4, on the fits to the beamstrahlung function, by comparing the results of such fits with the data whence they stem.

For each collider configuration considered in sect. 4 there are two figures (that correspond to the second and third line of eq. (28), and to the fourth line of that equation, respectively), each of which has two panels (that correspond to the y_+ and y_- variables). All panels have the same layout, composed of a main frame and a lower inset (note, however, that the domain and codomain ranges are generally different across the various figures). In the main frame the GuineaPig data (including their error bars; data are normalised to their total number, hence the label “frequency”), are displayed as magenta points, while the fit result is shown as a piecewise continuous green line; the inset shows the ratio of the quantities that appear in the main frame, in the form data over fit.

References

- [1] J. Alwall, R. Frederix, S. Frixione, V. Hirschi, F. Maltoni, O. Mattelaer et al., *The automated computation of tree-level and next-to-leading order differential cross sections, and their matching to parton shower simulations*, *JHEP* **07** (2014) 079, [1405.0301].
- [2] C. Degrande, C. Duhr, B. Fuks, D. Grellscheid, O. Mattelaer et al., *UFO - The Universal FeynRules Output*, *Comput.Phys.Commun.* **183** (2012) 1201–1214, [1108.2040].
- [3] J. Alwall, A. Ballestrero, P. Bartalini, S. Belov, E. Boos et al., *A Standard format for Les Houches event files*, *Comput.Phys.Commun.* **176** (2007) 300–304, [hep-ph/0609017].
- [4] J. Butterworth, A. Arbey, L. Basso, S. Belov, A. Bharucha et al., *The Tools and Monte Carlo working group Summary Report*, 1003.1643.
- [5] J. Alwall, M. Herquet, F. Maltoni, O. Mattelaer and T. Stelzer, *MadGraph 5 : Going Beyond*, *JHEP* **1106** (2011) 128, [1106.0522].

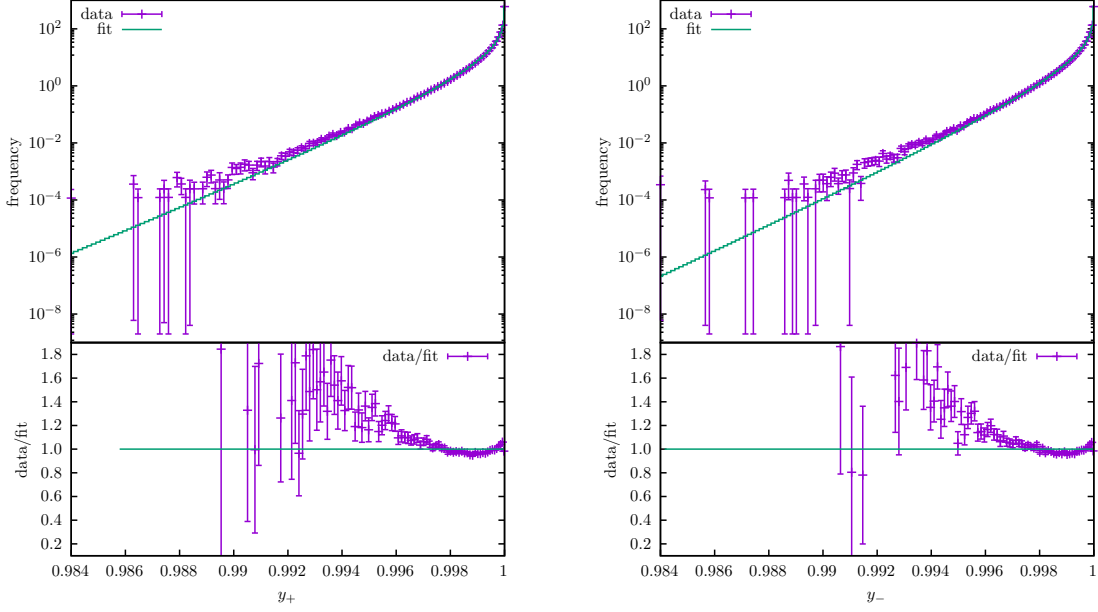


Figure 1: Fits to the second (left panel) and third (right panel) of eq. (28), for FCC-ee240.

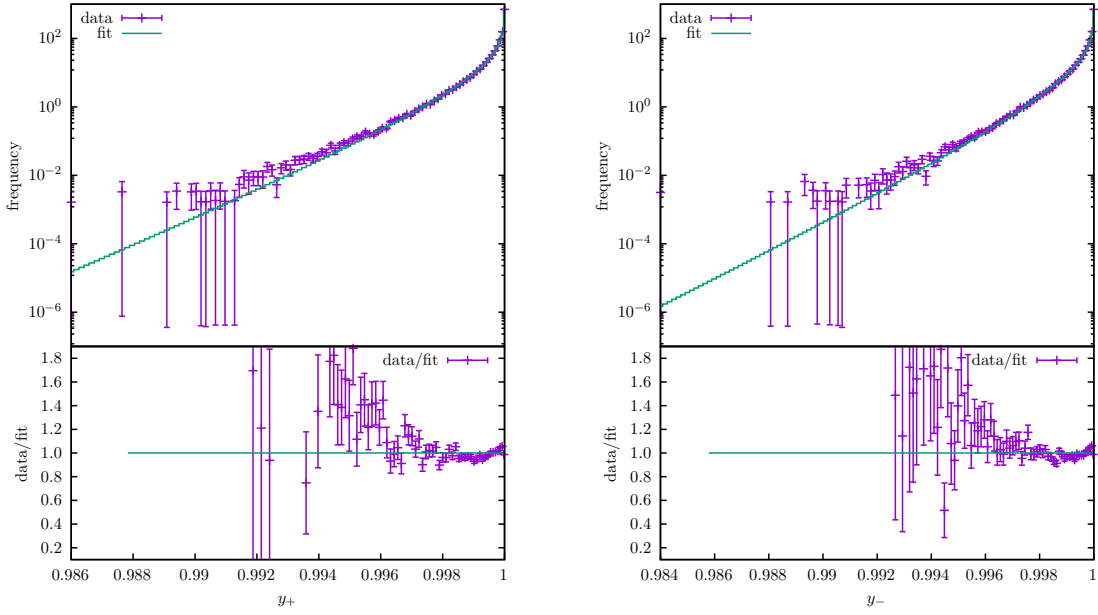


Figure 2: Fits to the y_+ (left panel) and y_- (right panel) components of the fourth line of eq. (28), for FCC-ee240.

- [6] R. Frederix, S. Frixione, F. Maltoni and T. Stelzer, *Automation of next-to-leading order computations in QCD: The FKS subtraction*, *JHEP* **0910** (2009) 003, [0908.4272].
- [7] S. Frixione, Z. Kunszt and A. Signer, *Three jet cross-sections to next-to-leading order*, *Nucl.Phys.* **B467** (1996) 399–442, [hep-ph/9512328].

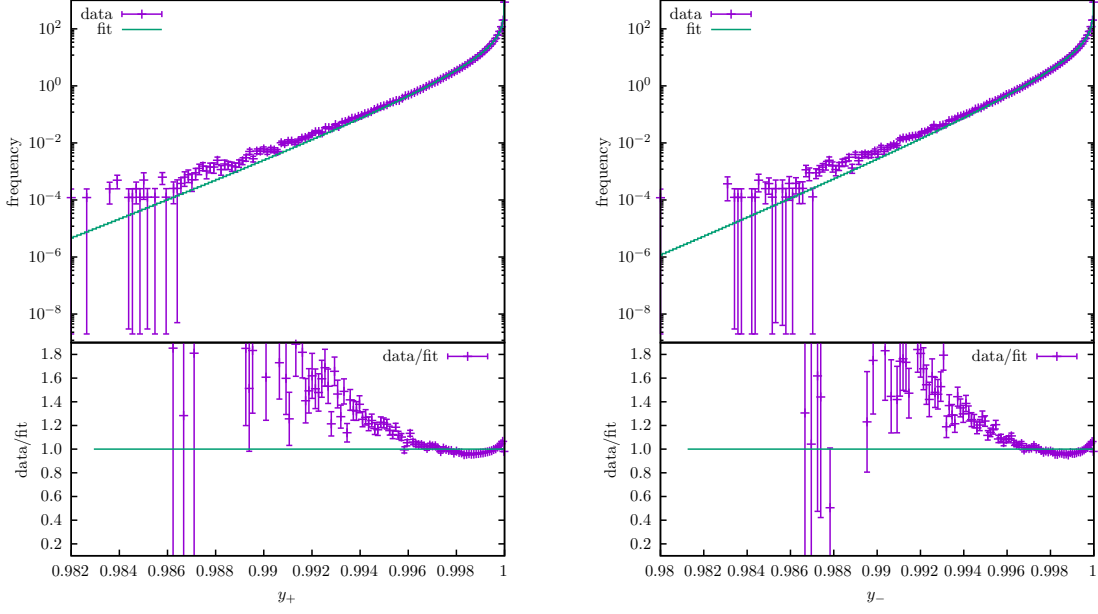


Figure 3: As in fig. 1, for FCC-ee365.

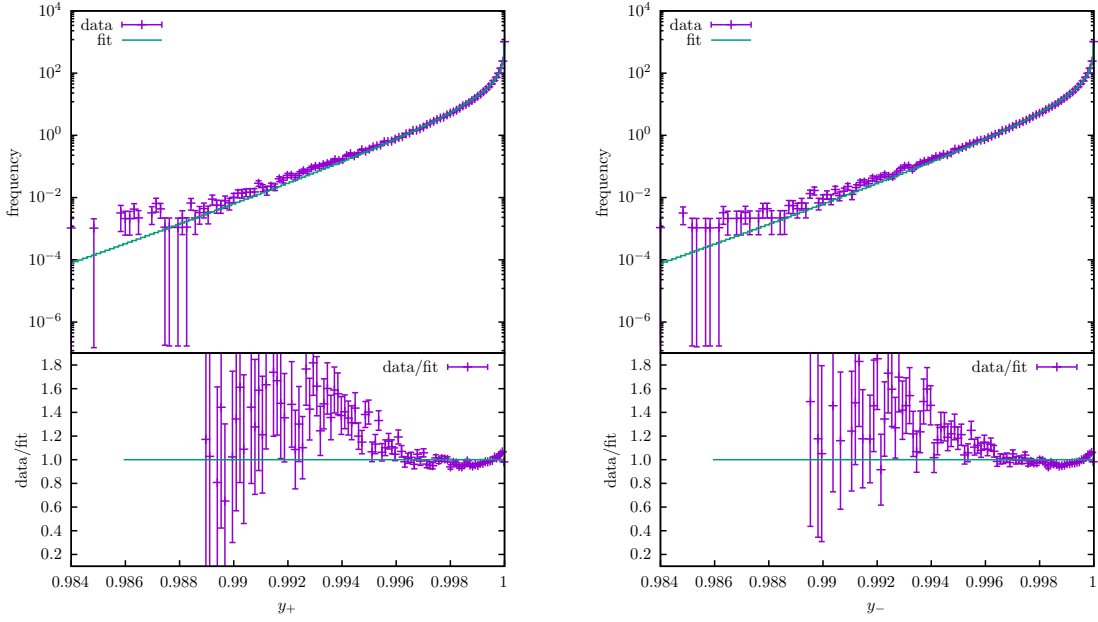


Figure 4: As in fig. 2, for FCC-ee365.

- [8] S. Frixione, *A General approach to jet cross-sections in QCD*, *Nucl.Phys.* **B507** (1997) 295–314, [[hep-ph/9706545](#)].
- [9] S. Frixione and B. R. Webber, *Matching NLO QCD computations and parton shower simulations*, *JHEP* **0206** (2002) 029, [[hep-ph/0204244](#)].

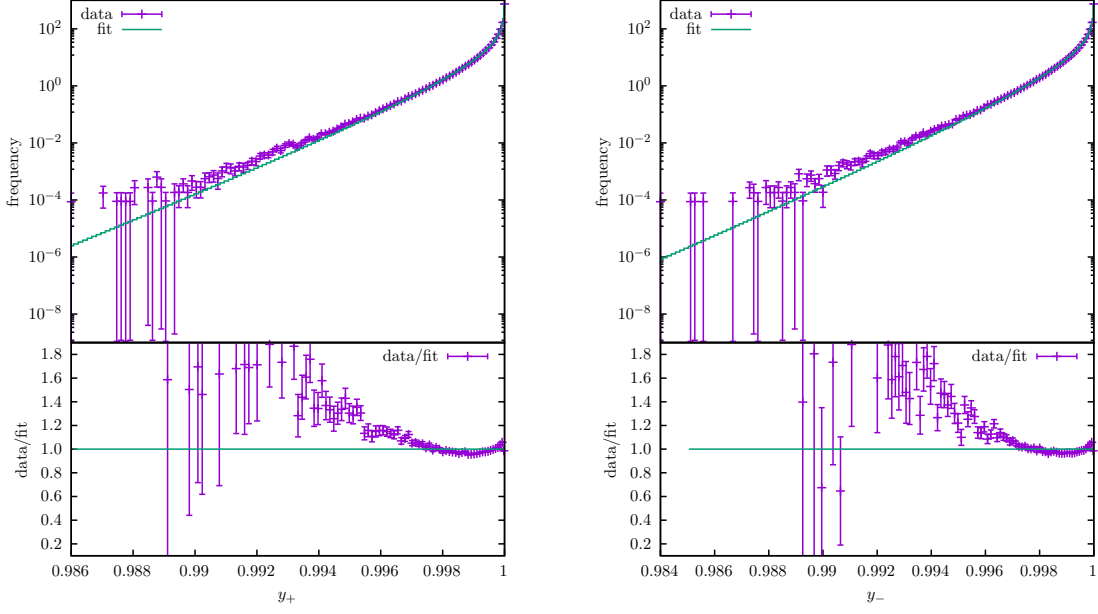


Figure 5: As in fig. 1, for CEPC240.

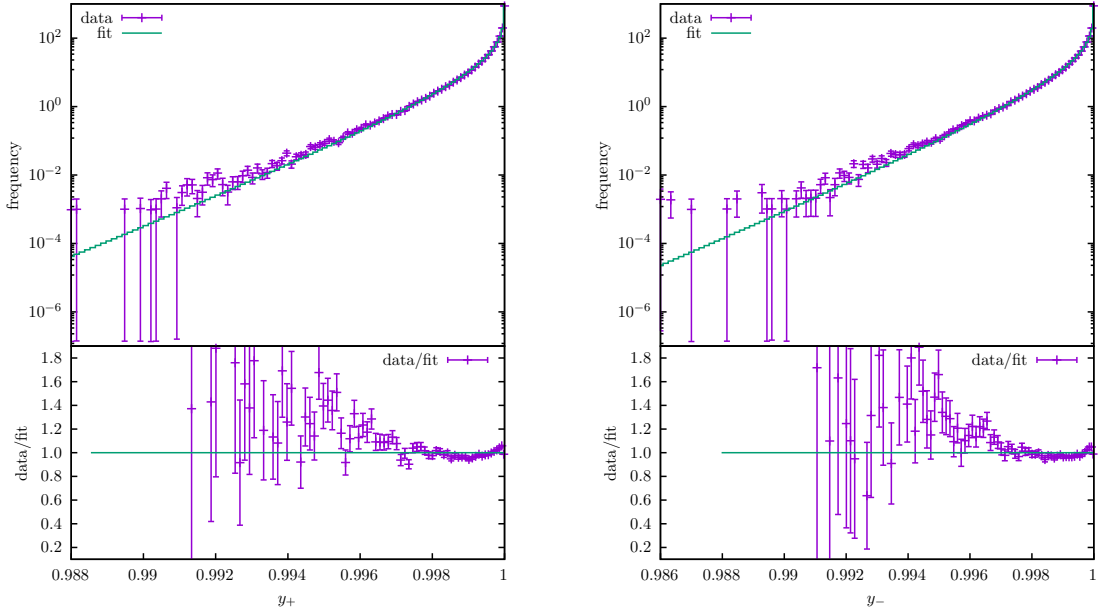


Figure 6: As in fig. 2, for CEPC240.

- [10] R. Frederix and S. Frixione, *Merging meets matching in MC@NLO*, *JHEP* **1212** (2012) 061, [[1209.6215](#)].
- [11] R. Frederix, S. Frixione, V. Hirschi, D. Pagani, H. S. Shao and M. Zaro, *The automation of next-to-leading order electroweak calculations*, *JHEP* **07** (2018) 185, [[1804.10017](#)].

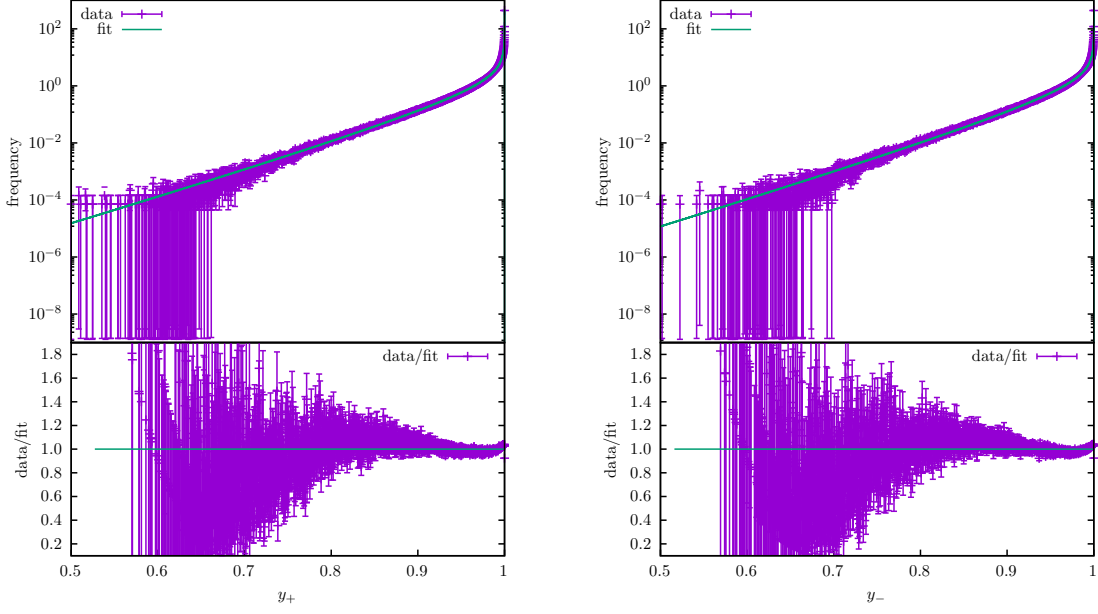


Figure 7: As in fig. 1, for ILC250.

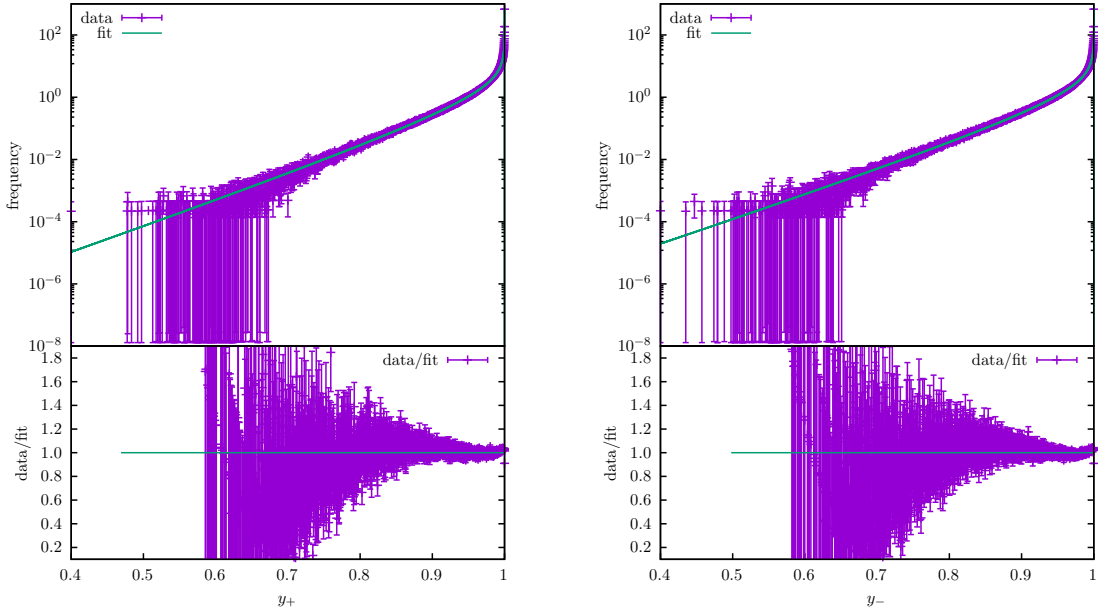


Figure 8: As in fig. 2, for ILC250.

- [12] C. Chen, Z. Cui, G. Li, Q. Li, M. Ruan, L. Wang et al., *H* \rightarrow e^+e^- at CEPC: ISR effect with MadGraph, 1705.04486.
- [13] Q. Li and Q.-S. Yan, *Initial State Radiation Simulation with MadGraph*, 1804.00125.
- [14] S. Frixione, *Initial conditions for electron and photon structure and fragmentation*

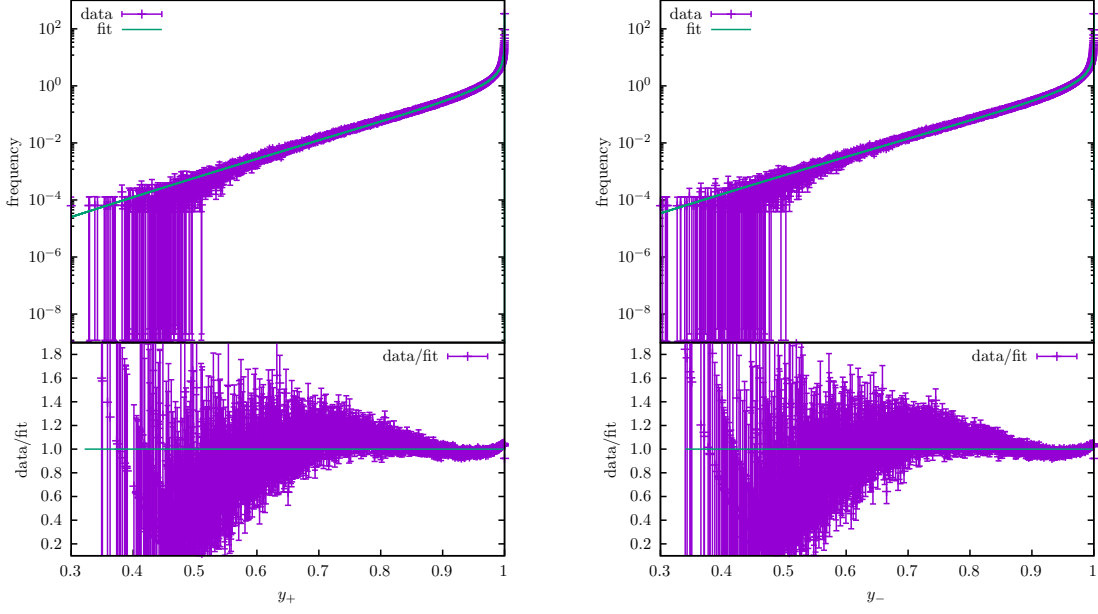


Figure 9: As in fig. 1, for ILC500.

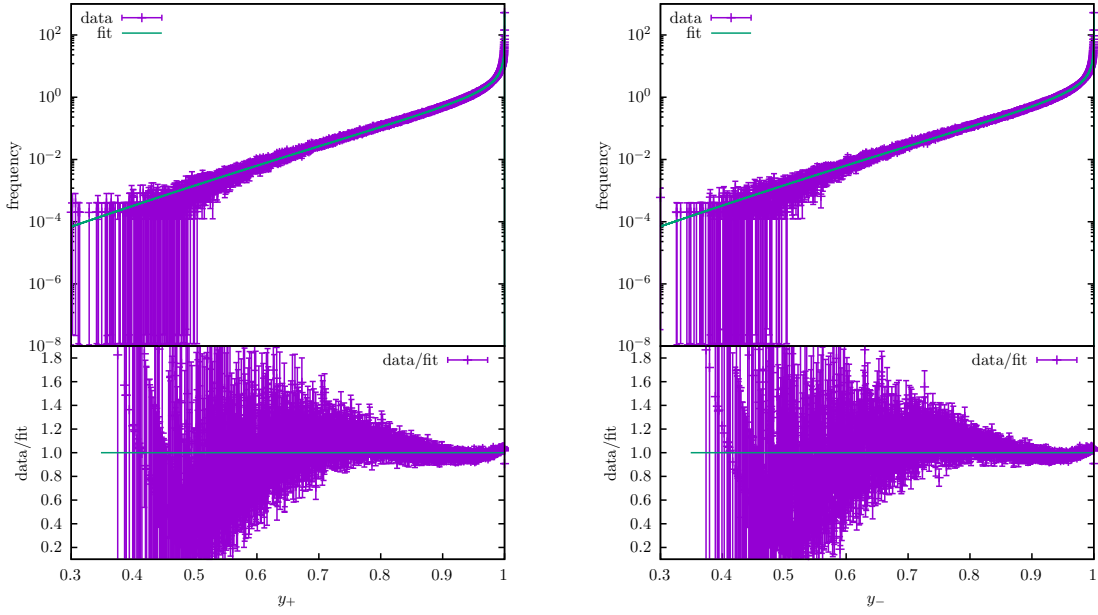


Figure 10: As in fig. 2, for ILC500.

functions, *JHEP* **11** (2019) 158, [1909.03886].

[15] V. N. Gribov and L. N. Lipatov, *Deep inelastic $e p$ scattering in perturbation theory*, *Sov. J. Nucl. Phys.* **15** (1972) 438–450.

[16] L. N. Lipatov, *The parton model and perturbation theory*, *Sov. J. Nucl. Phys.* **20** (1975)

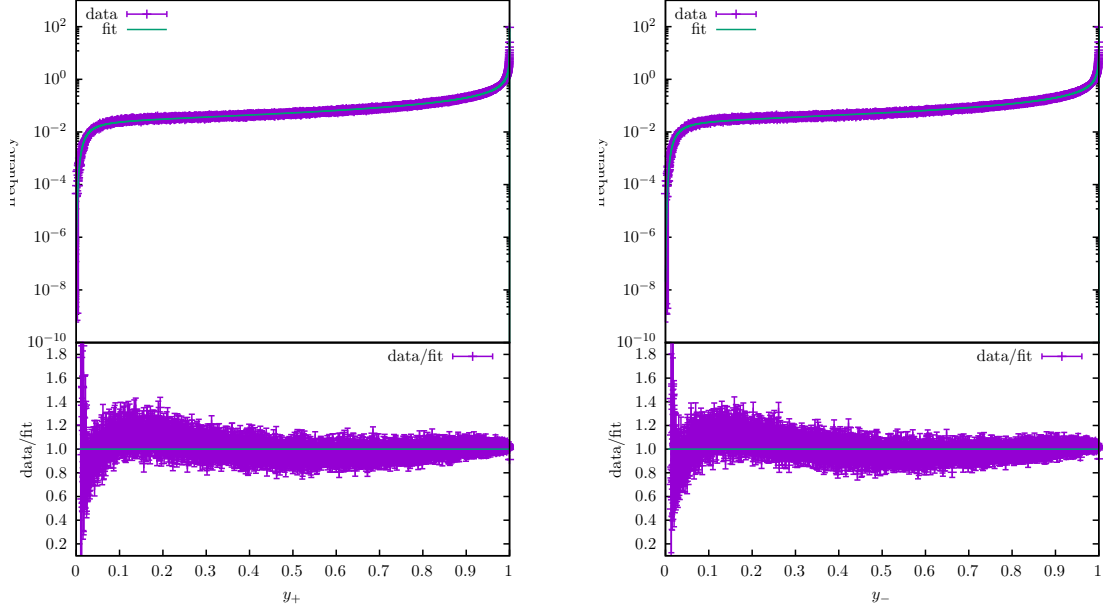


Figure 11: As in fig. 1, for CLIC3000.

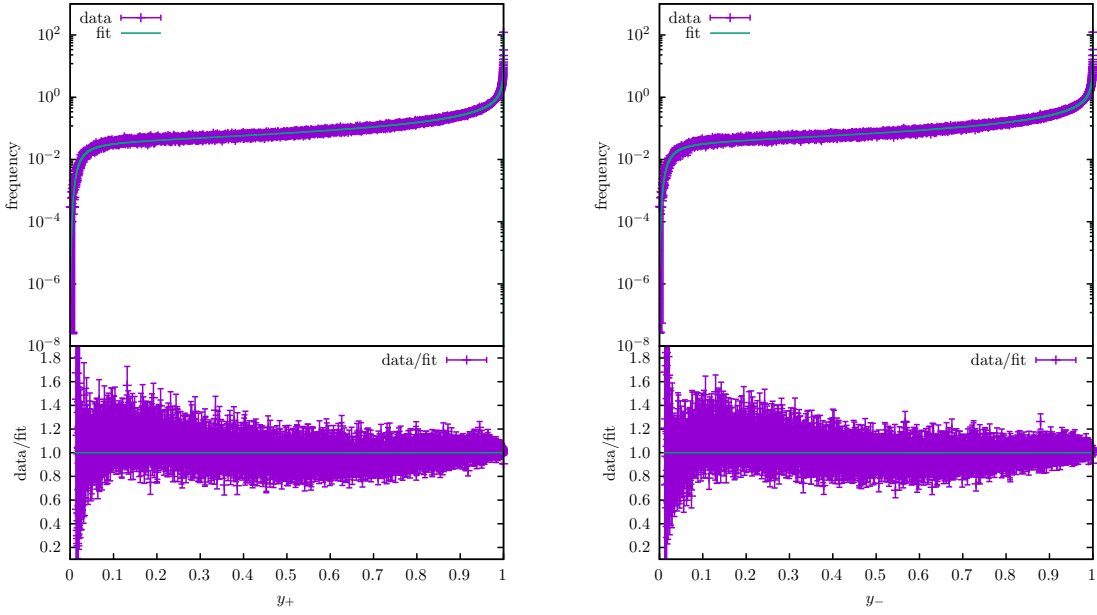


Figure 12: As in fig. 2, for CLIC3000.

94–102.

- [17] G. Altarelli and G. Parisi, *Asymptotic Freedom in Parton Language*, *Nucl. Phys.* **B126** (1977) 298–318.
- [18] Y. L. Dokshitzer, *Calculation of the Structure Functions for Deep Inelastic Scattering and*

- e+ e- Annihilation by Perturbation Theory in Quantum Chromodynamics.*, *Sov. Phys. JETP* **46** (1977) 641–653.
- [19] M. Skrzypek and S. Jadach, *Exact and approximate solutions for the electron nonsinglet structure function in QED*, *Z. Phys.* **C49** (1991) 577–584.
 - [20] M. Skrzypek, *Leading logarithmic calculations of QED corrections at LEP*, *Acta Phys. Polon.* **B23** (1992) 135–172.
 - [21] M. Cacciari, A. Deandrea, G. Montagna and O. Nicrosini, *QED structure functions: A Systematic approach*, *Europhys. Lett.* **17** (1992) 123–128.
 - [22] V. Bertone, M. Cacciari, S. Frixione and G. Stagnitto, *The partonic structure of the electron at the next-to-leading logarithmic accuracy in QED*, *JHEP* **03** (2020) 135, [1911.12040].
 - [23] S. Frixione, *On factorisation schemes for the electron parton distribution functions in QED*, 2105.06688.
 - [24] F. Maltoni and T. Stelzer, *MadEvent: Automatic event generation with MadGraph*, *JHEP* **0302** (2003) 027, [hep-ph/0208156].
 - [25] P. Chen, G. Horton-Smith, T. Ohgaki, A. W. Weidemann and K. Yokoya, *CAIN: Conglomerat d’ABEL et d’interactions nonlineaires*, *Nucl. Instrum. Meth. A* **355** (1995) 107–110.
 - [26] D. Schulte, *Study of Electromagnetic and Hadronic Background in the Interaction Region of the TESLA Collider*. PhD thesis, Hamburg U., 1997.
 - [27] C. Rimbault, P. Bambade, O. Dadoun, G. Le Meur, F. Touze, M. C. del Alabau et al., *GUINEA PIG++ : An Upgraded Version of the Linear Collider Beam Beam Interaction Simulation Code GUINEA PIG*, *Conf. Proc. C* **070625** (2007) 2728.
 - [28] T. Ohl, *CIRCE version 1.0: Beam spectra for simulating linear collider physics*, *Comput. Phys. Commun.* **101** (1997) 269–288, [hep-ph/9607454].
 - [29] A. P. Sailer, *Studies of the measurement of differential luminosity using Bhabha events at the International Linear Collider*. PhD thesis, Humboldt U., Berlin, 2009. 10.3204/DESY-THESIS-2009-011.
 - [30] W. Kilian, T. Ohl and J. Reuter, *WHIZARD: Simulating Multi-Particle Processes at LHC and ILC*, *Eur. Phys. J. C* **71** (2011) 1742, [0708.4233].
 - [31] K. Yokoya and P. Chen, *Electron Energy Spectrum and Maximum Disruption Angle Under Multi-Photon Beamstrahlung*, *Conf. Proc. C* **8903201** (1989) 1438.